

Galaxy Deblending using Residual Dense Neural networks

Hong Wang

*Stony Brook University, Stony Brook, NY 11794 and
Computational Science Initiative, Brookhaven National Laboratory, Upton, NY 11973*

Sreevarsha Sreejith and Anže Slosar

Physics Department, Brookhaven National Laboratory, Upton, NY 11973

Yuewei Lin and Shinjae Yoo

Computational Science Initiative, Brookhaven National Laboratory, Upton, NY 11973

(Dated: September 21, 2021)

We present a new neural network approach for deblending galaxy images in astronomical data using Residual Dense Neural network (RDN) architecture. We train the network on synthetic galaxy images similar to the typical arrangements of field galaxies with a finite point spread function (PSF) and realistic noise levels. The main novelty of our approach is the usage of two distinct neural networks: i) a *deblending network* which isolates a single galaxy postage stamp from the composite and ii) a *classifier network* which counts the remaining number of galaxies. The deblending proceeds by iteratively peeling one galaxy at a time from the composite until the image contains no further objects as determined by classifier, or by other stopping criteria. By looking at the consistency in the outputs of the two networks, we can assess the quality of the deblending. We characterize the flux and shape reconstructions in different quality bins and compare our deblender with the industry standard, **SExtractor**. We also discuss possible future extensions for the project with variable PSFs and noise levels.

I. INTRODUCTION

Astronomical survey science is entering a decade which will witness a surfeit of new optical imaging data that will transform astronomical and cosmological research. The new datasets obtained from upcoming ground-based and space-based observing facilities will image vast areas of the sky at unprecedented depths. Among the most important of these will be the Legacy Survey of Space and Time (LSST) from the Vera Rubin Observatory [1], which will complement not only the already existing datasets from Dark Energy Survey (DES, [2]) and Hyper-Suprime Cam (HSC,[3]), but also the data from upcoming space-based surveys like Euclid [4]. Due to the large field of view, most of these surveys will not be able to employ adaptive optics resulting in an arcsec sized point spread function (PSF). At the depths of these surveys, this will result in blending, affecting over half of the galaxies in the survey (for example, in [5], the authors estimate that approximately 60% of the objects in the HSC are affected by this problem).

Blending, especially if undetected, can introduce serious systematic errors in the survey analysis. These include potentially catastrophically wrong inference of fluxes, leading to biased photometric redshifts, biased estimates of shear and local object density dependent systematics that can interact with galaxy and cluster detections. The main approach to solving the blending problem is two-pronged. On one hand, there is the realization that source separation (deblending) will never be perfect and we should focus on understanding its properties and its effects on the analysis. This is done through simulations and artificial source injections into real data. On

the other hand, the better the deblender we have, the smaller the corrections we need to do to make our analysis unbiased. We therefore need both good deblenders and good schemes for understanding their imperfections.

Deblending is in principle a well defined problem. The basic model is that the images of individual galaxies are combined on the projected plane, assuming perfect transparency (i.e. intensities add), and then observed through the atmosphere and telescope with known PSF and noise properties. The most sophisticated deblenders on the market combine machine-learning approaches for setting priors on galaxy shapes, and physical modelling for things that we can model explicitly, like the noise and the PSF [6, 7].

Several machine-learning based methods have been proposed recently, in order to grapple with the galaxy deblending problem. [8] designed a branched deblender with generative adversarial networks, which can work on the deblending of images with two overlapped galaxies. [9] developed a framework for measuring the photometry of blended galaxies as well as perform segmentation with a standard convolutional neural network (CNN) and a U-Net. In 2020, [5] introduced an algorithm where a Variational Auto Encoder(VAE)-like neural network was used for galaxy deblending. Most of the current generation neural-network based galaxy deblenders require the galaxy to be located at the center of the image in order to give the network a sign as to which galaxy to recover, which is often impractical and prevents the model from being used iteratively, i.e., it will degrade the model's performance on the image after the first galaxy is removed. Besides, the number of galaxies in the blended image for the previous methods is always fixed, and to the best of

our knowledge, there is no neural network based galaxy deblending framework that can work on images with an arbitrary and unknown number of galaxies. In this paper, we propose an innovative deblending framework with a galaxy deblender, and a classifier that can deblend galaxies from a blended image iteratively without any prior information about the number of galaxies. In addition, since the deblender recovers galaxies based on their luminosity, our framework has no constraint on the position of the galaxies. Nevertheless, like other machine-learning approaches to deblending, our work remains exploratory as we aim to better understand the applicability of neural networks to astronomical image analysis.

This paper is organized as follows: in Section II, we introduce the architecture of our framework including the deblender and the classifier, and the experimental settings used to train the model. In Section III, we present the experimental results and the comparison with the industry standard deblending method - Source Extractor (SExtractor, [10]). The discussion and conclusion follow, in the last Section IV.

II. NEURAL NETWORK ARCHITECTURE AND TRAINING

A. Proposed Framework

Our goal is to deblend galaxies from astronomical images with an arbitrary and unknown number of overlapped galaxies. The proposed framework consists of two components: a *deblender*, which isolates the image corresponding to a single galaxy from an astronomical image, and a *classifier*, which counts how many galaxies remain in the image. The *deblender* and *classifier* are then used iteratively to separate the scene into its constituent galaxy images. This is illustrated in the Figure 1 and represented in the following meta-code:

```
while True:
    num_galaxies = classifier(image)
    if num_galaxies == 0:
        exit loop
    deblended_galaxy = deblender(image)
    image -= deblended_galaxy
```

Specifically, given a noisy blended image with multiple galaxies, the deblender will take it as the input and output a noiseless image with a single galaxy as it is trained. This single-galaxy image is then subtracted from the input of the deblender to get the residual image which is another noisy blended image. The classifier is used to determine if there are further galaxies in the residual image, and if there are, this process is repeated until there is no galaxy left in the residual image.

In an ideal case, the classifier will detect one fewer galaxy at each step and the process will stop when there are no more galaxies left. We call such deblends *High*

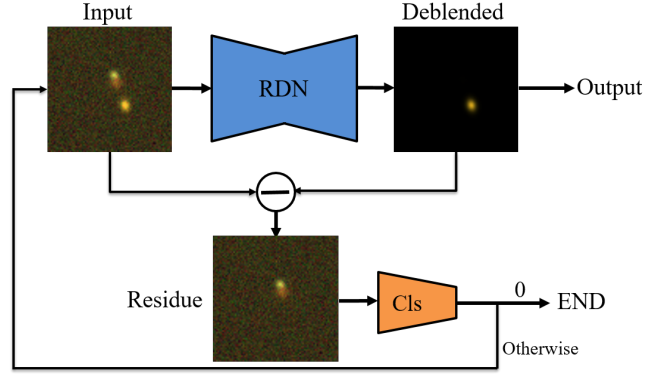


FIG. 1: Framework.

quality deblends. In a non-ideal case, one of the two following scenarios often play out. The number of galaxies in the image does not decrease by one galaxy per iteration, but the process still eventually comes to a halt with zero galaxies detected in the final image. When this happens, we refer to the result as *Medium quality* deblends. The third case is if the process gets stuck in an infinite loop where the *classifier* maintains that there are more than zero galaxies in the image, but the deblender fails to locate them. Then, if the classifier predicts the same non-zero number of galaxies in the residual image for three consecutive iterations we terminate the iteration and call the results *Low quality* deblends.

The next subsection describes the architectures of our two main components.

B. Deblender

Given an astronomical image with multiple overlapped galaxies, the deblender aims to deblend one galaxy from it. A Residual Dense Network (RDN) [11] is trained as the deblender in this framework. RDN shows superior performance in image super-resolution [11] and image restoration [12]. For the deblending task, the RDN will take noisy blended images with multiple galaxies as input and the output will be a noiseless image containing the brightest galaxy.

Figure 2 shows the architecture of the RDN, starting with a shallow feature extraction net (SFTNet), which includes two convolutional layers that extract features from the input. The SFTNet is followed by the main component of the RDN, namely the residual dense blocks (RDBs). Each RDB contains C convolutional layers with a ReLU activation function. The layers in the RDB are densely connected, which means the feature maps from all the preceding layers of the current RDB as well as the output from the preceding RDB will be the input of the current convolutional layer. The feature maps from the convolutional layers in the current RDB and the preceding RDB are also concatenated as a local feature fusion, followed by a 1×1 convolutional layer. At the end of

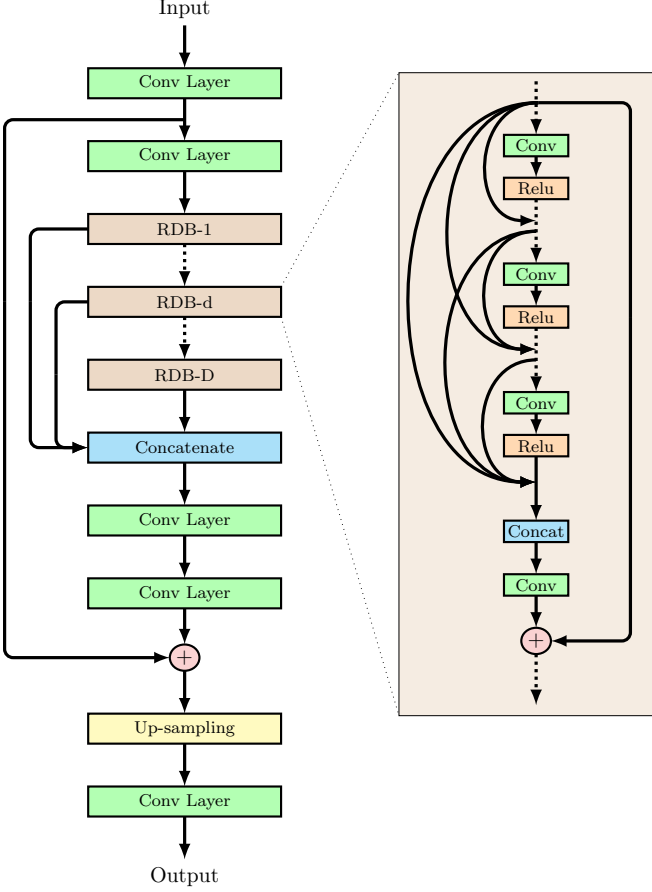


FIG. 2: The architecture of RDN.

an RDB, there is a local residual step by the addition of the output from the previous RDB. Following D RDBs, where D denotes the number of RDBs, is a global feature fusion where, similar to the local feature fusion, the features from all the RDBs will be concatenated and then passed to a 1×1 convolutional layer. The last step before the up-sampling net is global residual learning, referring to an addition between the current features and the features from the first convolutional layer in SFTNet. The efficient sub-pixel convolutional neural network (ESPCN) followed by a convolutional layer forms the up-sampling net. Since the RDN in our framework is used for deblending, the output image will have the same size as the input image. During training, the RDN will take noisy blended images as input and predict noiseless images with a single galaxy. ℓ_1 -norm is used to compute the difference between the output of the RDN and the ground truth, thus the loss function for RDN is written:

$$\ell_{\text{RDN}}^{\theta}(I, I_{gt}) = \frac{1}{WH} \sum_{x=1}^W \sum_{y=1}^H |f(I, \theta)_{x,y} - (I_{gt})_{x,y}| \quad (1)$$

where I is the input noisy blended image and $f_{\theta}(I)$ is the output of the RDN with θ referring to the parameters

in the model. I_{GT} denotes the ground truth image, which is a noiseless image with the brightest galaxy.

In Figure 2 we show a schematic representation of the *deblender* network.

C. Classifier

For the classifier portion of the deblending network, we use a VGG-16 network [13]. VGG-16 contains 13 convolutional layers and 3 fully connected layers. In our framework, it is modified to have four classes as output, i.e., the classifier can tell if the images have 0, 1, 2 or 3 galaxies.

In the first phase of training, the classifier is trained on images with galaxies ranging from 0 to 3. During the second phase in the training process where the deblender and the classifier are trained jointly, the deblended images from the deblender will also be passed through the classifier to see if the RDN has deblended only one galaxy from the blended image. This loss will also be used to update the RDN's parameters. Thus, the training set of the classifier contains both noiseless and noisy images with 0 to 3 galaxies. The cross-entropy (CE) loss is utilized to train the classifier parameterized by ϕ as Eq. 2 where y represents the one-hot ground truth label.

$$\ell_{CE}^{\phi}(I) = -y^T \cdot \log(g(I, \phi)) \quad (2)$$

D. Training & Test Data

In this work, we use BlendingToolKit [14] in order to simulate the galaxy images and to generate the blended images. BlendingToolkit is a complete framework whose functionalities include generation of images with blended objects as well as providing measurements of the deblending and detection performance. It relies on the industry standard `galsim` [15] packages to make the actual renderings of the galaxies and is built on top of the `WeakLensingDeblending` [16] package.

We first generate noiseless images of single galaxies, which can be considered as the pre-blended ground truth images. We employ the LSST DM galaxy catalog with a span of 1 square deg (`OneDegSq.fits` supplied with the BlendingToolKit). We use the default options, which impose a magnitude cut on the i -band, $i < 25.3$. Then, the noiseless blended images are generated by a pixelwise summation between these single galaxy images. Additional random Poisson noise is added to the image to get the noisy blended images corresponding to the LSST 10-year depth. We selected g , r and i bands from the resultant images and converted them into RGB images. The original dimension of the generated images is (120, 120, 3). We crop each image to (80, 80, 3) from the center. The pixel values of the blended images will be normalized to $[0, 1]$ before entering the framework and the

pre-blended images will be scaled to $[-1, 1]$ following [8].

Unlike the other machine learning based deblending methods where one of the galaxies has to be located at the center of the image [8, 9], there is no constraint on the positions of the galaxies for our deblender, because we train it to output the object with the highest luminosity. This is also the reason why our framework can work iteratively. The use of the summation when creating the blended images also makes the iterative process possible. During training, the noisy blended images are treated as the input and the noiseless image with the brightest galaxy as the pre-blended ground truth for the deblender. Our goal is to train a deblender that can deblend and denoise at the same time and will always recover the brightest galaxy from the blended images. The classifier is trained with 0–3 galaxies and for each of the four classes, half of the training data contain noiseless images while the other half contain noisy images. This is essential in order to train a classifier that can tell the number of galaxies in both noiseless and noisy images at the same time.

We generate 50,000 2-galaxy blended images with BlendingToolKit as the training set for the deblender. The test set contains 1000 blended images with 2 galaxies in each. There is also a second test set with 1000 3-galaxy blended images, to demonstrate the generalization of our framework. For the classifier, we generated blended images containing 0, 1, 2 and 3 galaxies, where each of the classes has 100,000 images (making it 400,000 in total), half of which are noiseless images and the other half noisy. The test set for the classifier contains 2000 images for each class and 8000 in total. The test set for the classifier also has the same ratio of noiseless and noisy images. Therefore, the classifier gives 4 classes as output indicating the number of galaxies in the input image.

E. Training procedure

The training process can be divided into two phases. In the first phase, the deblender and the classifier are pre-trained separately until they perform reasonably. Then they are fine-tuned jointly to boost the performance of both, while working in the iterative setting. Specifically, we expect that the classifier will force the deblender to output only one galaxy, while the deblender will provide more intermediate images to motivate the classifier to have better discrimination ability.

During the pre-training of the RDN, the noisy two-galaxy blend images are used as the input and the noiseless images with the brighter single galaxy as the ground truth. Eq. 1 is the objective function during this process. A model trained in this way will have the ability to not only deblend the brighter galaxy, but also to denoise simultaneously. Meanwhile, in the first training phase the classifier is trained on the dataset containing both noisy and noiseless blended images with 0, 1, 2 and

3 galaxies. This pre-training phase makes the trained classifier able to classify both noisy and noiseless images and the trained RDN to determine the end of the whole workflow. They will be used during together during the second phase of the training.

During the second phase, the deblender and the classifier will be trained jointly. The framework will operate as it is designed, i.e., the deblender will be run twice because the input contains two galaxies. The blended image, denoted as I_{blend} will be passed through the deblender to get the deblended $I_{\text{deblend-1}}$, which is compared with the ground truth $I_{\text{gt-1}}$ to build the ℓ_1 -norm loss $l_{\text{RDN}}(I_{\text{deblend-1}}, I_{\text{gt-1}})$. The first residual image $I_{\text{res-1}}$ is the subtraction between I_{blend} and $I_{\text{deblend-1}}$. Generally, the residual images are fainter than the blended images and therefore they will be normalized by dividing with the maximum pixel values. Then, the deblender will predict and scale back to recover the second galaxy $I_{\text{deblend-2}}$ from $I_{\text{res-1}}$ and another residual image $I_{\text{res-2}}$ will be calculated. For simplicity, we use $\mathbb{S} = \{I_{\text{blend}}, I_{\text{deblend-1}}, I_{\text{deblend-2}}, I_{\text{res-1}}, I_{\text{res-2}}, I_{\text{gt-1}}, I_{\text{gt-2}}\}$ to denote all the images. In this phase, the classifier will be optimized by all the available images in \mathbb{S} as formulated in Eq. 3. Since \mathbb{S} is class-imbalanced with more 1-galaxy images than 0 and 2-galaxy images, α_I is used as a weight. For 1-galaxy images, $\alpha_I = 0.2$, otherwise $\alpha_I = 1$. For the deblender, in addition to $l_{\text{RDN}}(I_{\text{deblend-1}}, I_{\text{gt-1}})$, it is updated based on a loss from the classifier's prediction on the deblended images. The objective function for the second phase can be formulated as Eq. 4. λ here is a trade-off coefficient.

$$l_{\text{phase-2}}^{\phi} = \sum_{I \in \mathbb{S}} \alpha_I l_{CE}(I) \quad (3)$$

$$l_{\text{phase-2}}^{\theta} = l_{\text{RDN}}(I_{\text{deblend-1}}, I_{\text{gt-1}}) + \lambda l_{CE}(I_{\text{deblend}}) \quad (4)$$

III. RESULTS

A. Experimental settings

1. Implementation details

The RDN used in our framework contains $D = 16$ RDBs with $C = 8$ convolutional layers in each block. During the first phase of the training process, the learning rate for the RDN is 10^{-4} , the batch size is 128, and it is trained for 150 epochs. For the classifier, the initial learning rate is 0.1, the batch size is 200, and it is trained for 200 epochs. In the second phase, the deblender and the classifier are updated jointly, where the learning rate decays to 10^{-5} for the former and 10^{-6} for the latter. After some experimentation, we chose the trade-off coefficient $\lambda = 10^{-4}$. The batch size is 8 due to GPU limit and the framework is trained for 10 epochs in this phase.

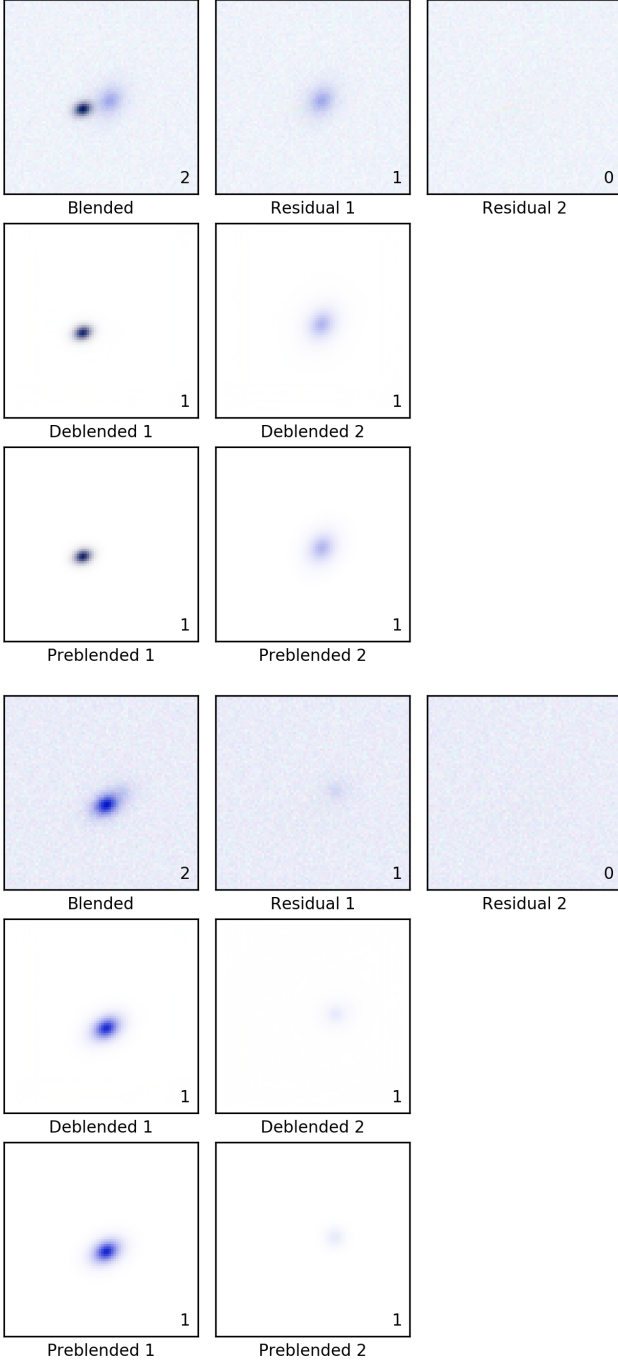


FIG. 3: Iterative results for 2-galaxy blended images. We show two examples. In each example, the top row shows the noisy image as it progresses through the iterative process with the input image on the left and the remaining noise image (after the galaxies were subtracted) on the right. The middle row show the galaxy images that were isolated from the input image by the *deblender*. The bottom row shows the ground truth, which can be visually compared with the deblended images above. All the images were plotted with inverse fluxes to improve the contrast (i.e. white corresponds to zero flux). The number at the corner of each image represents the number of remaining galaxies as determined by the classifier.

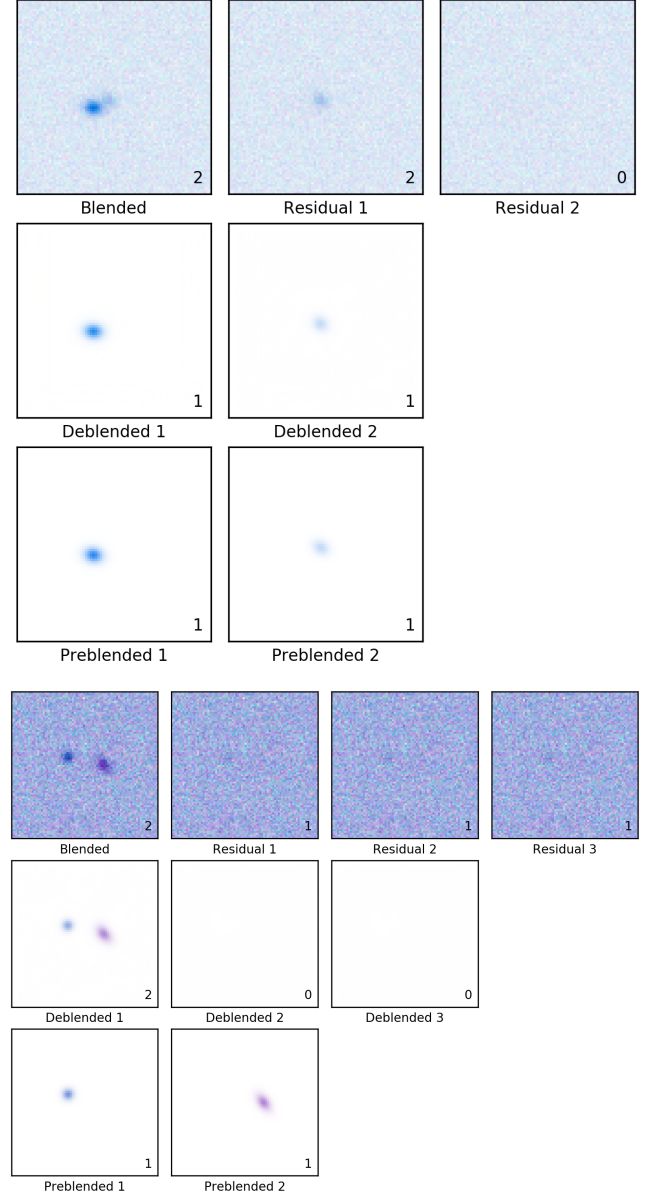


FIG. 4: As Fig. 3, but for medium and low quality samples.

2. Evaluation

We trained the framework on 2-galaxy blended images and tested the trained model on both 2-galaxy and 3-galaxy blended images. Both test sets contain 1000 noisy blended images.

We start by showing some example results in Figures 3 and 5. These results show the typical output from a high-quality deblend. The network is using both the morphological as well as the color information to isolate images of individual galaxies which is helpful in recovering images even in difficult cases.

In Table I we present the fraction of deblends sorted by

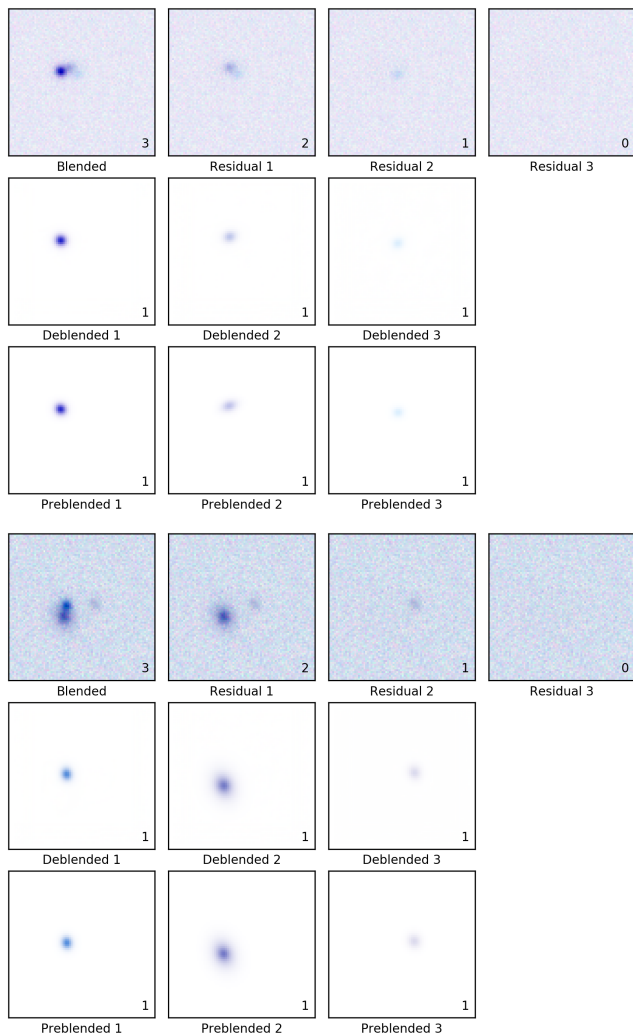


FIG. 5: As Fig. 3, but for 3 galaxy blends.

TABLE I: Iterative test on 2-galaxy and 3-galaxy blended images.

	2-galaxy	3-galaxy
High-quality	77.3%	50.4%
Medium-quality	15.3%	36.9%
Low-quality	7.4%	12.7%

the quality category (see Section II A) for 2-galaxy and 3-galaxy problems. Note that this only indicates how well the scheme thinks it is doing, rather than how well it is actually doing. With this caveat, the process shows relatively good results with a large fraction of nominally high-quality deblends.

To quantify the quality of the deblends, we start with some standard image analysis metrics. We applied the peak signal-to-noise ratio (PSNR) and the structural similarity index (SSIM) as metrics to evaluate the quality of deblended images from the deblender when compared with the ground truth.

PSNR represents a peak error in the measurement of reconstruction quality in image compression. It computes the logarithm of the ratio between the maximum pixel value (MAX) of the ground truth and the mean squared error (MSE) between the test image and the ground truth in decibels. In our experiment, the ground truth consists of noiseless images with a single galaxy and the test images are the corresponding deblended images from the RDN. PSNR is formulated as Eq. 5:

$$\text{PSNR}(\text{dB}) = 20 \cdot \log_{10}(\text{MAX}) - 10 \cdot \log_{10}(\text{MSE}) \quad (5)$$

SSIM [17], known as the structural similarity index, is commonly used to evaluate the similarity between two images using the means μ_x and μ_y , the variances σ_x and σ_y and the covariance σ_{xy} . In Eq. 6, $c_1 = (k_1 L)^2$ and $c_2 = (k_2 L)^2$ are two small constants to avoid the instability with a weak denominator. We use $k_1 = 0.01$, $k_2 = 0.03$ by default and L is the dynamic range of pixel values.

$$\text{SSIM} = \frac{(2\mu_x\mu_y + c_1)(2\sigma_{xy} + c_2)}{(\mu_x^2 + \mu_y^2 + c_1)(\sigma_x^2 + \sigma_y^2 + c_2)} \quad (6)$$

Results are summarized in Table II. We do observe a few trends here. First, the PSNR of the second deblended galaxy is higher than that of the first. This somewhat counter-intuitive result comes from the normalization of PSNR, since the second deblend is fainter than the first one. In other words, the PSNR is not telling us that the 2nd deblended galaxy is better deblended, only that its quality is less degraded than expected, given how much fainter it is. This interpretation is confirmed by the SSIM values, which are higher for the first deblend, but only marginally. In both cases we see that the 3-galaxy problem is more difficult than the 2-galaxy problem. We also see that the median values are systematically above the mean values, telling us that the mean is pulled down by a small number of catastrophic outliers. To study these results in language that is more relevant to the astronomy community, we turn to the recovery of the fluxes and moments, described in the next section.

B. Flux and image moment recovery using RDN

An important measure of the effectiveness of any algorithm such as ours is the accurate recovery of physical parameters from the input image. To that end, we have opted to compare the fluxes and the second order image moments (which represent the equivalent ellipse of the image and by extension, the shape and orientation) retrieved by the RDN against that of the truth images. For ease of reference, the brighter galaxies in each field are referred to as ‘x’ galaxies and the fainter ones as ‘y’ galaxies.

Figure 6 shows a comparison of the fluxes of the x galaxies as recovered by the RDN against the truth images for the test set. The larger panel on the left shows

	2-galaxy problem				3-galaxy problem			
	PSNR		SSIM		PSNR		SSIM	
	Mean	Median	Mean	Median	Mean	Median	Mean	Median
Deblended 1	56.51	57.93	0.9973	0.9997	54.66	57.19	0.9954	0.9997
Deblended 2	58.18	59.02	0.9967	0.9997	55.96	58.77	0.9929	0.9996
Deblended 3					57.71	59.29	0.9956	0.9995

TABLE II: PSNR(dB) and SSIM for 2-galaxy and 3-galaxy deblending problems.

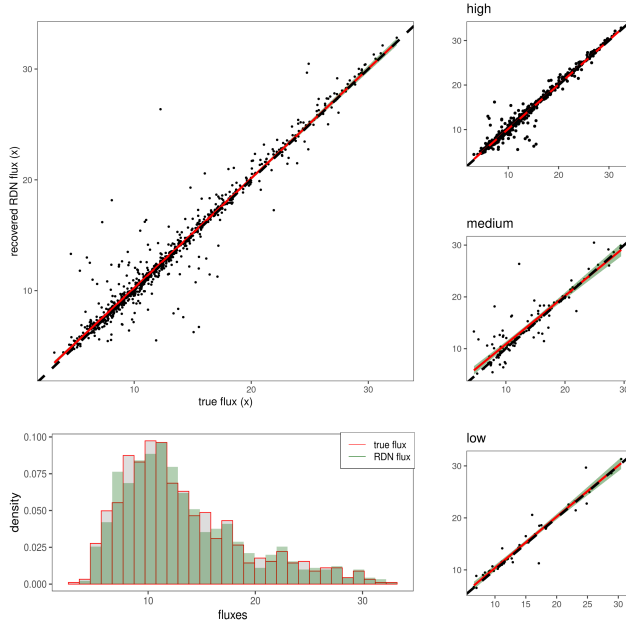


FIG. 6: Plot showing the comparison of the fluxes recovered from the RDN and the true fluxes for the x galaxies. The red line is the linear regression fit to the data and the dashed black line is an arbitrary $y = x$ fit. The shading in green denotes a 95% confidence interval to the linear fit.

the true fluxes on the X-axis and the RDN fluxes on the y-axis. The solid red line is a linear regression fit to the data, and the dashed black line is an arbitrary $y = x$ fit. The light green shading represents a 95% confidence interval to the linear fit. The three smaller panels on the right side show the same fits to the high, medium and low quality blends which are detailed in Section II A. The overlapping histograms in the bottom left panel show the density distributions of the RDN and true fluxes. Figure 7 is a similar representation for the fainter, y galaxies.

As is evident from Figure 6, the RDN is very efficient in recovering the fluxes for the brighter galaxies in our fields, more or less uniformly so for the high, medium and low quality images. The effectiveness of the RDN for this group of images can be further observed from the overlapping histograms of the true (red) and recovered (green) fluxes in the bottom left panel. Figure 7 shows the same plots for the fainter, y galaxies. As ex-

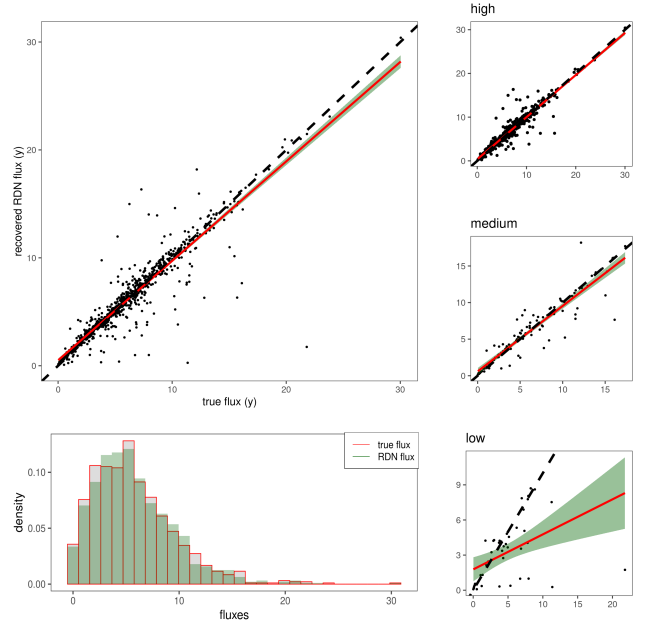


FIG. 7: As Fig. 6, but for the y galaxies.

pected, the lower quality assignments are associated with a higher scatter between real and measured fluxes, although for the brighter galaxy, there is no measurable difference between the medium and low quality marks (given the size of our test catalog). For the fainter galaxies, however, the low quality deblends are essentially uncorrelated with the true values. We find that except for secondary objects in the low-quality bin, our RDN based estimator is essentially unbiased in recovering flux values.

Similarly to the fluxes, the shapes and orientations of the galaxies, represented by their second order image moments, are crucial characteristics that we aimed to recover using the RDN, in particular with the weak lensing application in mind. Figure 8 shows a comparison of the moment μ_{11} for the truth images and the RDN recovered images. The bigger panels show the true moment on the x-axis and the RDN recovered moment on the y-axis for the x and y galaxies. The blue line is an arbitrary $y = x$ fit. The smaller panels on the bottom show the same plot for the high, medium and low quality images. Results for the other component of the second order moment, $\mu_{20} - \mu_{02}$ looks qualitatively the same. In an ideal deblender, the results would lie on the $y = x$ line, but we

notice the appearance of a curious cross, which we will comment on below.

Figure 9 shows a comparison of the second order moments (μ_{11} , $\mu_{20} - \mu_{02}$) plotted against each other for both the ground truth x and y galaxies (green) with the moments recovered by the RDN superimposed (blue). We see no evidence of any preferred axis in the recovered distribution of these quantities.

This leads to a curious result. The ensemble properties of the RDN recovered fluxes are correctly distributed. However, the per-galaxy results have structure that goes beyond the normal scatter around the truth result. In particular, the cross seen in Figure 8 implies that galaxies with a significant μ_{11} sometimes end up having zero recovered μ_{11} , but also vice-versa, that galaxies with zero true μ_{11} occasionally end up having a significant recovered μ_{11} .

One plausible explanation for this curious result is as follows. In Figure 10 we plot the histogram of the truth value of $|\mu_2| = \sqrt{(\mu_{20} - \mu_{02})^2 + (2\mu_{11})^2}$, i.e. the rotationally invariant measure of the non-circularity of the image. This histogram shows a distinct peak at around $\mu = 0$ region. The simulated galaxies fall into two classes, those that are approximately round and those which are not. The RDN network seems to have learned this and tries to classify the galaxy into one of the two categories before reconstructing its image. The arms of the crosses correspond to these failures: one for the non-circular galaxies reconstructed as circular ones and the other for the circular galaxies reconstructed as the non-circular ones.

C. Comparison with SExtractor

In this section, we compare our deblending strategy with what is widely considered as the industry standard, Source Extractor (SExtractor, [10]), which has been the baseline detection, deblending and image extraction software in astronomy for over two decades. It returns a set of user specified parameters from the more extensive default parameter file, by following the specific configurations defined by the user. In this work, we have used the Python formulation of SExtractor, *sep* [18] with the settings employed for DES[19].

We note that this is a fundamentally unfair comparison for several reasons. First, the RDN has been trained for this particular set of galaxies and thus internally employs a correctly tuned prior for the distribution of morphologies, fluxes and ellipticities, while SExtractor employs a general algorithm and is thus intrinsically more robust. Moreover, following DES configuration, SExtractor is run on the co-added image (R+G+B) and is thus missing the color information. Nevertheless, it is an appropriate sanity check to measure what kind of improvements can be brought about by employing more sophisticated methods.

Figure 11 shows the comparison of the flux recovery by

the RDN and SExtractor for both the x and y galaxies. The top left and right panels feature the RDN recovered and SExtractor recovered fluxes on the y -axis and the true fluxes on the X -axis for the x galaxies. The bottom left and right panels are the same representations for the y galaxies. The red line is a linear regression fit to the data, with the light green shading representing a 95% confidence interval. The dashed black line shows $y = x$. As is evident from the plots, the RDN does a better job of recovering the object fluxes for both the x and y galaxies. SExtractor has a tendency to put a disproportionate amount of flux into the first detected objects, and hence the x images are biased high, while the y images are biased low.

Measuring moments for SExtractor images is considerably more difficult due to the presence of noise in them and the results are overly noisy. Correctly subtracting the noise contribution in a fair manner goes beyond the scope of this paper.

D. Failure modes

In this section we investigate the most common failure modes in the two approaches by cherry-picking cases, in which one method performs correctly while the other fails.

We manually looked at all the cases where RDN detects just a single galaxy. In a majority of those, the secondary object was very faint and overlapped almost perfectly with the primary, leading to the deblending being suspended because the *classifier* determined that there are no further objects. However, for 12 out of the 1000 objects in the test set, for the deblended x galaxies, the result clearly shows two objects, examples of which are shown in Figure 13. These problems are trivial for the SExtractor approach. A visual inspection of all these images was conducted and it was observed that, both the objects in 7 of these fields are very similar in shape and, in 5 fields, they had similar brightnesses. It stands to reason that the RDN has some difficulty in deblending objects with similar structural parameters, most likely because it cannot decide which is the “brighter” object, especially in the presence of noise. In fact, when presented with such examples in training, it simply pays a large loss penalty whenever it starts with the “wrong” object, without a clear rule about how to pick one of the two objects if the noise hides the identity of the bright ones. We will discuss this further in Section IV.

When SExtractor is run on the test set, it returns photometric parameters for 979 x galaxies and 729 y galaxies (the x counterparts of all y galaxies are present in the x set). As seen in Figure 13, this includes 9 instances where the RDN fails to deblend the different galaxies in the field. However, overall, there are more instances where the RDN successfully deblends the x and y galaxies, while SExtractor either doesn’t detect either galaxy, or only detects the x galaxy, but not the y galaxy,

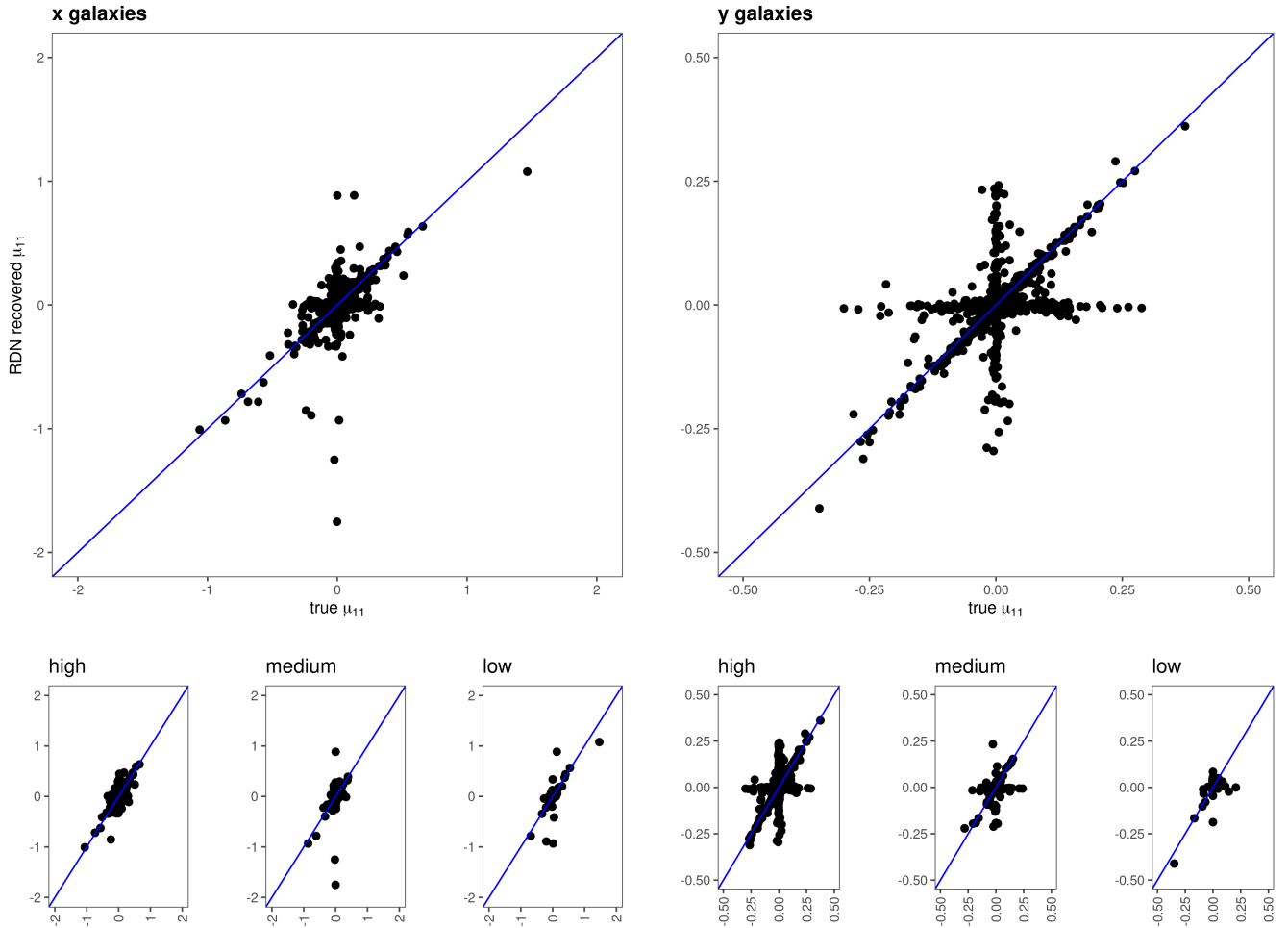


FIG. 8: Plot showing the comparison of true μ_{11} and RDN recovered μ_{11} for the brighter (x) and the fainter (y) galaxies on the large top plots. The smaller second row plots show the same split by quality bin. The blue line is a $y = x$ fit.

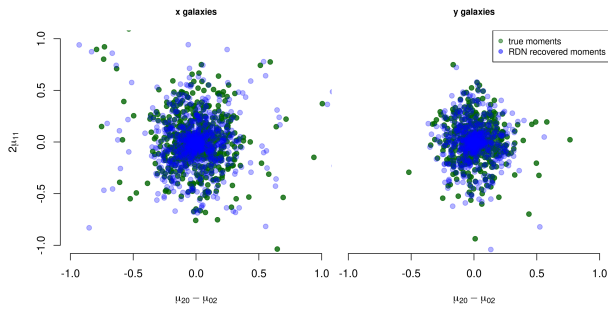


FIG. 9: Plot showing the second order image moments for x and y ground truth images in green, with the RDN recovered moments superimposed in blue. The true and recovered moments exhibit the same general distribution while some scatter is observed at the edges of the plot.

a few examples of which are illustrated by Figure 14. We note that these are traditional blend merges, where the deblender merges two distinct objects into a single one. Since human eye is pretty good at detecting these, we could possibly improve upon this by fine-tuning the SExtractor settings, potentially at the cost of artificially shredding objects with substructure. These are also examples where color information is most helpful.

IV. SUMMARY AND CONCLUSIONS

In this work we present a new approach to deblending using a Residual Dense Network, which was trained on blended galaxy images with a realistic PSF and noise levels, and which has performed decently in deblending and recovering object fluxes and shapes. Compared to previous works, our set up does not assume that the object to be deblended is located at the center of the image. We

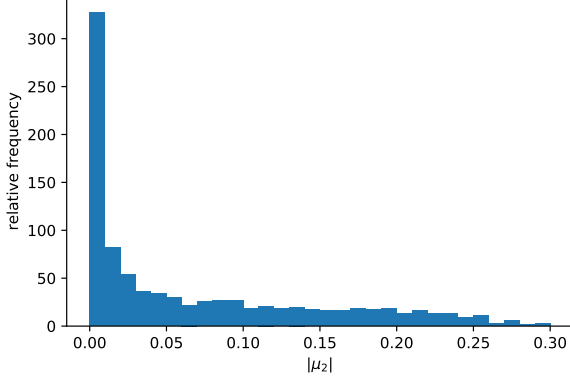


FIG. 10: Plot showing the histogram of the absolute value of the second moment $|\mu_2|$ for the true images. The true simulated galaxies belong to two categories: they are either round $|\mu_2| = 0$ or not. The histogram is truncated with a small number of galaxies with considerably higher $|\mu_s|$ s.

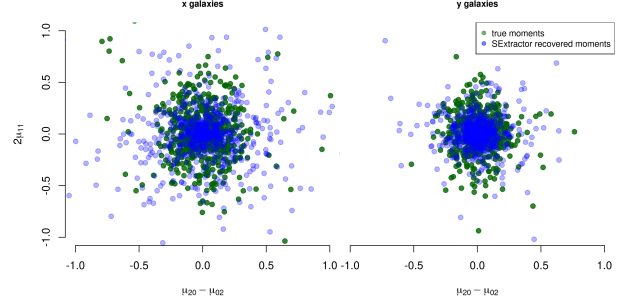


FIG. 12: Plot showing the second order image moments for x and y ground truth images in green, with the SExtractor recovered moments superimposed in blue. While the distribution is similar to that in Figure 9, the SExtractor recovered moments exhibit much larger scatter than the RDN recovered moments.

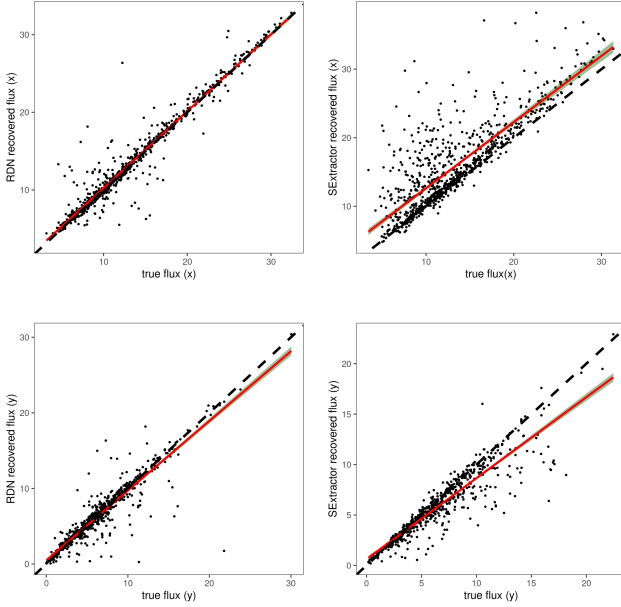


FIG. 11: Plot showing the comparison of flux recovery from the RDN and SExtractor. The top left and right panels show the true fluxes on the X-axis and the RDN and SExtractor fluxes on the y-axis respectively for x galaxies. The red line is a linear regression fit with a 95% confidence interval represented by light green shading. The dashed black line is the $y = x$ line. The bottom left and right panels are the same representations for y galaxies.

also do not need to assume in advance, the number of objects to be deblended. By using two neural networks, one to perform deblending and one to determine the number of remaining objects in the field, we can classify the quality of deblends. We have shown that deblends that are designed to be higher quality have indeed, less noisy fluxes and shapes.

In the most current deblending networks found in literature, the network is trained to deblend the central galaxy. Given that centering in the presence of noise presents its own problems, we have trained our network to deblend the brightest galaxy remaining in the image. This works very well, where the choice of the brightest is clear, but leads to a particular failure mode where the network cannot decide where to start, when two objects are approximately equally bright (see Figure 13). This might be a generic feature of any kind of deblender that proceeds by peeling off one galaxy at a time. For example, even if we choose the galaxy closer to the center, there would likely be an equivalent failure mode when two galaxies are equally close to the center. The same thing could happen for other initial assumptions that attempt to distinguish between the galaxies. There are several approaches to solve this. One possibility would be to use a symmetrized loss function that would train the network to deblend either galaxy. Another possibility would be to have a more sophisticated network that deblends multiple galaxies at once, perhaps again with an appropriately symmetrized loss function.

We have found that our method outperforms the industry standard SExtractor on flux recovery, subject to strong caveats mentioned in the Section III C. However, we found that the RDN recovered shapes are either very good or catastrophically wrong. The catastrophic failures result in the cross-effect discussed in Section III B. One possible explanation for this involves bimodality in the shapes of the truth objects and the RDN internally assigning the image to the wrong class. It also serves as a warning for use of a deeply non-linear deblender based

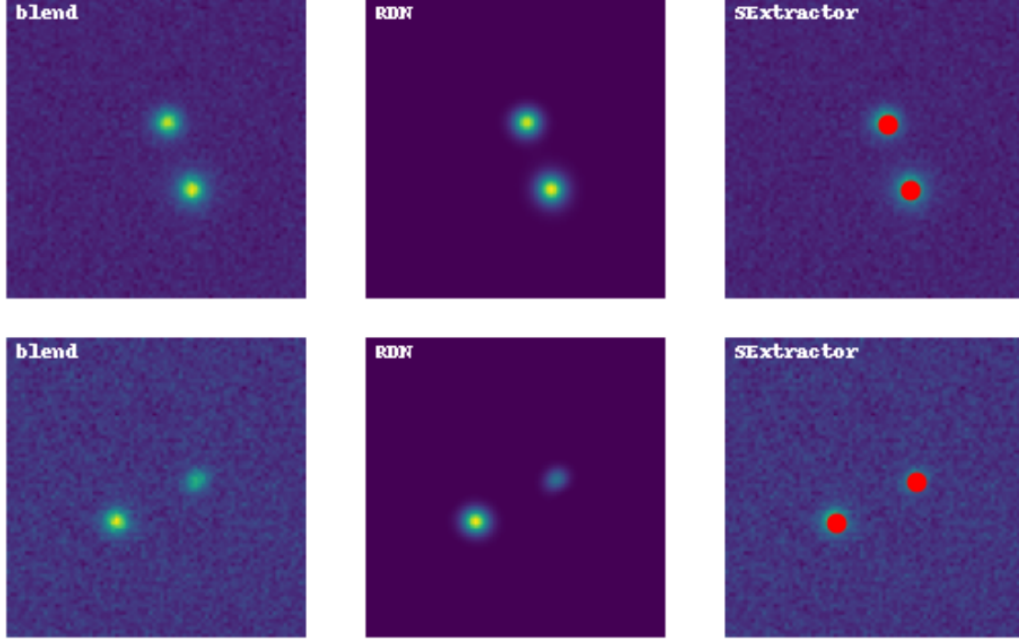


FIG. 13: Instances where the RDN fails, while SExtractor succeeds in detecting and deblending the objects in the field. On the left is the original blend, in the centre is the output of the RDN and on the right is the blend with the SExtractor detections superimposed in red.

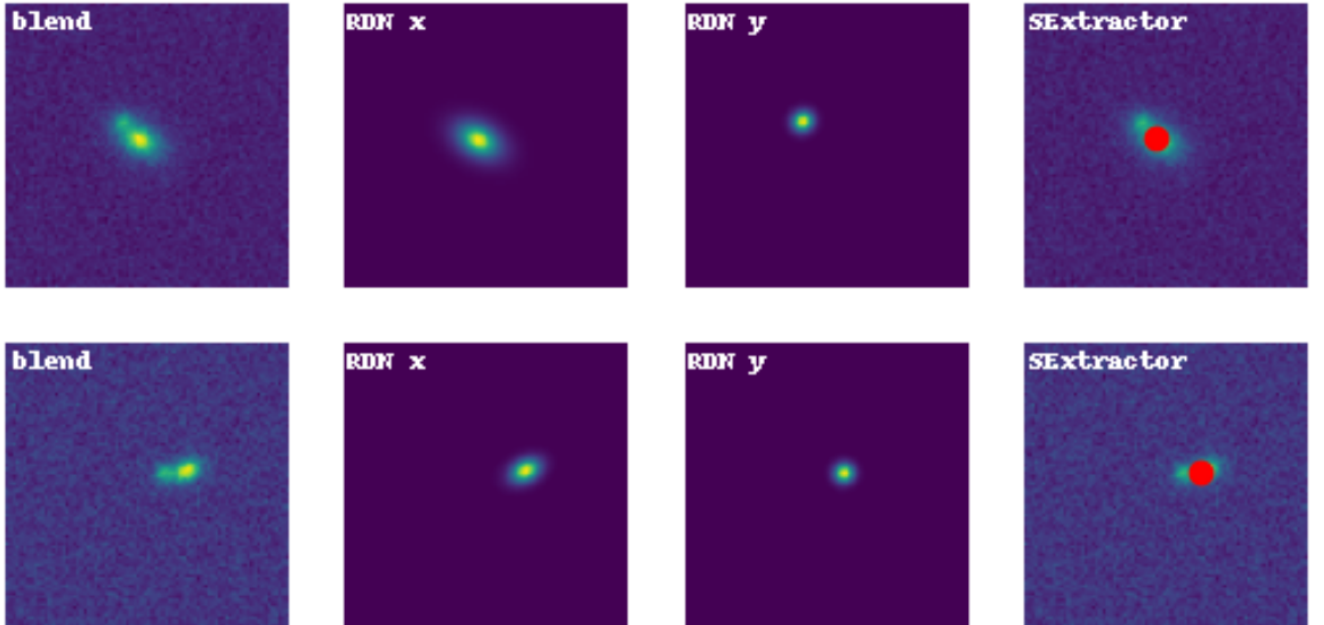


FIG. 14: Instances where SExtractor fails to detect and deblend, while the RDN succeeds. On the far left is the original blend, the RDN result is represented in the two central panels for the x and y galaxies, and the blend with the SExtractor detection superimposed in red is on the far right panel.

on NN for work requiring precision shapes, such as weak lensing. At the same time, such work could lead to potentially interesting new work on galaxy-star separation and morphological classification of galaxies.

Similarly to the majority of other neural network approaches, our deblender cannot deal optimally with a PSF that is variable and is different for the different input channels (for e.g. for different bands), nor can it deal with a pixel mask. This is a significant deficiency that is usually swept under the rug under the assumption that the network can be retrained for a set of different PSF. However, in practice, we have a different PSF for different bands and with the typical astronomical observations in five or six bands, the number of possible PSF combinations becomes unmanageable. The PSF shape in each band thus needs to be part of the input and network training. We are leaving these important aspects for future work.

One of the main advantages of most ML approaches to deblending is that they also automatically denoise and deconvolve the image and can in principle fill in the missing information in case of pixel masks. For a sufficiently

sophisticated neural network, this would trivialize many typical operations such as flux and shear estimation on the resulting truth images. However, it would also require us to have a more advanced way of propagation of both statistical and systematic uncertainties.

This work has demonstrated the feasibility of using RDN in astronomical image analysis and has highlighted some of the unresolved issues with the current machine learning approaches to the deblending problem in the case of realistic astronomical images.

ACKNOWLEDGEMENTS

This material is based upon work supported by the U.S. Department of Energy, Office of Science, Office of Advanced Scientific Computing Research through the SciDAC grant “Accelerating HEP Science: Inference and Machine Learning at Extreme Scales”. We thank our collaborators for useful input.

-
- [1] LSST Science Collaboration, P. A. Abell, J. Allison, S. F. Anderson, J. R. Andrew, J. R. P. Angel, L. Armus, D. Arnett, S. J. Asztalos, T. S. Axelrod, and et al., LSST Science Book, Version 2.0, arXiv e-prints , arXiv:0912.0201 (2009), arXiv:0912.0201 [astro-ph.IM].
 - [2] T. M. C. Abbott, F. B. Abdalla, A. Alarcon, J. Aleksić, S. Allam, S. Allen, A. Amara, J. Annis, J. Asorey, S. Avila, and et al., Dark Energy Survey year 1 results: Cosmological constraints from galaxy clustering and weak lensing, *Phys. Rev. D* **98**, 043526 (2018), arXiv:1708.01530 [astro-ph.CO].
 - [3] C. Hikage, M. Oguri, T. Hamana, S. More, R. Mandelbaum, M. Takada, F. Köhlinger, H. Miyatake, A. J. Nishizawa, H. Aihara, R. Armstrong, J. Bosch, J. Coupon, A. Ducout, P. Ho, B.-C. Hsieh, Y. Komiyama, F. Lanusse, A. Leauthaud, R. H. Lupton, E. Medezinski, S. Mineo, S. Miyama, S. Miyazaki, R. Murata, H. Murayama, M. Shirasaki, C. Sifón, M. Simet, J. Speagle, D. N. Spergel, M. A. Strauss, N. Sugiyama, M. Tanaka, Y. Utsumi, S.-Y. Wang, and Y. Yamada, Cosmology from cosmic shear power spectra with Subaru Hyper Suprime-Cam first-year data, *PASJ* **71**, 43 (2019), arXiv:1809.09148 [astro-ph.CO].
 - [4] A. Refregier, A. Amara, T. D. Kitching, A. Rassat, R. Scaramella, and J. Weller, Euclid Imaging Consortium Science Book, arXiv e-prints , arXiv:1001.0061 (2010), arXiv:1001.0061 [astro-ph.IM].
 - [5] B. Arcelin, C. Doux, E. Aubourg, C. Roucelle, and LSST Dark Energy Science Collaboration, Deblending galaxies with variational autoencoders: A joint multiband, multi-instrument approach, *MNRAS* **500**, 531 (2021), arXiv:2005.12039 [astro-ph.IM].
 - [6] P. Melchior, F. Moolekamp, M. Jerdee, R. Armstrong, A. L. Sun, J. Bosch, and R. Lupton, SCARLET: Source separation in multi-band images by Constrained Matrix Factorization, *Astronomy and Computing* **24**, 129 (2018), arXiv:1802.10157 [astro-ph.IM].
 - [7] F. Lanusse, P. Melchior, and F. Moolekamp, Hybrid Physical-Deep Learning Model for Astronomical Inverse Problems, arXiv e-prints , arXiv:1912.03980 (2019), arXiv:1912.03980 [astro-ph.IM].
 - [8] D. M. Reiman and B. E. Göhre, Deblending galaxy superpositions with branched generative adversarial networks, *Monthly Notices of the Royal Astronomical Society* **485** (2019).
 - [9] A. Boucaud, C. Heneka, E. E. Ishida, N. Sedaghat, R. S. de Souza, B. Moews, H. Dole, M. Castellano, E. Merlin, V. Roscani, *et al.*, Photometry of high-redshift blended galaxies using deep learning, *Monthly Notices of the Royal Astronomical Society* **491**, 2481 (2020).
 - [10] E. Bertin and S. Arnouts, SExtractor: Software for source extraction., *A&AS* **117**, 393 (1996).
 - [11] Y. Zhang, Y. Tian, Y. Kong, B. Zhong, and Y. Fu, Residual dense network for image super-resolution, in *Proceedings of the IEEE conference on computer vision and pattern recognition* (2018) pp. 2472–2481.
 - [12] Y. Zhang, Y. Tian, Y. Kong, B. Zhong, and Y. Fu, Residual dense network for image restoration, *IEEE Transactions on Pattern Analysis and Machine Intelligence* (2020).
 - [13] K. Simonyan and A. Zisserman, Very deep convolutional networks for large-scale image recognition, arXiv preprint arXiv:1409.1556 (2014).
 - [14] <https://github.com/LSSTDESC/BlendingToolkit>.
 - [15] B. T. P. Rowe, M. Jarvis, R. Mandelbaum, G. M. Bernstein, J. Bosch, M. Simet, J. E. Meyers, T. Kacprzak, R. Nakajima, J. Zuntz, H. Miyatake, J. P. Dietrich, R. Armstrong, P. Melchior, and M. S. S. Gill, GALSIM: The modular galaxy image simulation toolkit, *Astronomy and Computing* **10**, 121 (2015), arXiv:1407.7676 [astro-

- ph.IM].
- [16] <https://github.com/LSSTDESC/WeakLensingDeblending>.
- [17] Z. Wang, A. C. Bovik, H. R. Sheikh, and E. P. Simoncelli, Image quality assessment: from error visibility to structural similarity, *IEEE transactions on image processing* **13**, 600 (2004).
- [18] K. Barbary, K. Boone, and C. Deil, Sep: V0.3.0 (2015).
- [19] <https://github.com/esheldon/sxdes>.